Neutral Pion Threshold Production at $Q^2 = 0.05$ GeV$^2/c^2$ and Chiral Perturbation Theory

H. Merkel,[1,*] P. Bartsch,[1] D. Baumann,[1] J. Bermuth,[2] A. M. Bernstein,[3] K. Bohinc,[4] R. Böhm,[1] N. Clawiter,[1]

S. Derber,[1] M. Ding,[1] M. O. Distler,[1] I. Ewald,[1] J. M. Friedrich,[1,†] J. Friedrich,[1] P. Jennewein,[1] M. Kahrau,[1]

M. Kohl,[5] K. W. Krygier,[1] M. Kuss,[5,‡] A. Liesenfeld,[1] P. Merle,[1] R. A. Miskimen,[6] U. Müller,[1] R. Neuhausen,[1]

M. M. Pavan,[3,§] Th. Pospischil,[1] M. Potokar,[4] G. Rosner,[1,∥] H. Schmieden,[1] M. Seimetz,[1] S. Širca,[4,¶]

A. Wagner,[1] Th. Walcher,[1] and M. Weis[1]

(A1 Collaboration)

[1]*Institut für Kernphysik, Johannes Gutenberg-Universität Mainz, D-55099 Mainz, Germany*
[2]*Institut für Physik, Johannes Gutenberg-Universität Mainz, D-55099 Mainz, Germany*
[3]*Laboratory for Nuclear Science, Massachusetts Institute of Technology, Cambridge, Massachusetts 02139*
[4]*Jožef Stefan Institute, SI-1001 Ljubljana, Slovenia*
[5]*Institut für Kernphysik, TU Darmstadt, D-64289 Darmstadt, Germany*
[6]*Department of Physics, University of Massachusetts, Amherst, Massachusetts 01003*
(Received 20 August 2001; published 20 December 2001)

New data are presented on the $p(e, e'p)\pi^0$ reaction at threshold at a four-momentum transfer of $Q^2 = 0.05$ GeV$^2/c^2$. The data were taken with the three-spectrometer setup of the A1 Collaboration at the Mainz Microtron MAMI. The complete center of mass solid angle was covered up to a center of mass energy of 4 MeV above threshold. Combined with measurements at three different values of the virtual photon polarization ϵ, the structure functions σ_T, σ_L, σ_{TT}, and σ_{TL} are determined. The results are compared with calculations in heavy baryon chiral perturbation theory and with a phenomenological model. The measured cross section is significantly smaller than both predictions.

Introduction.—Threshold electromagnetic pion production is a fundamental process since the pion is a "Goldstone boson," reflecting the spontaneously broken chiral symmetry of QCD [1]. In the chiral limit, where the quark and pion masses vanish, the *s* wave production amplitudes of neutral pions vanish. However, the explicit chiral symmetry breaking due to the small but finite quark mass ($m_u \approx 5$ MeV/c^2, $m_d \approx 9$ MeV/c^2) and finite pion mass render these amplitudes finite.

Calculations of these observables are performed by an effective field theory called chiral perturbation theory (ChPT) [1], which is generally in good agreement with experiment [2]. The systematic application of ChPT to reactions involving heavy baryons by Ref. [3] (heavy baryon chiral perturbation theory, HBChPT) has been generally successful in describing $\pi - N$ scattering and electromagnetic pion production from the nucleon.

In recent years there has been a considerable experimental effort to test this theoretical approach [2]. Of specific interest to this work, photo production experiments were performed at Mainz [4–6] and at SAL [7,8] and showed an impressive agreement with the predictions of Ref. [3]. These experiments were extended to finite photon four-momentum transfer $-Q^2$ via electroproduction at NIKHEF [9,10] and MAMI [11] at $Q^2 = 0.1$ GeV$^2/c^2$, which is believed to be the limit of the predictive power of HBChPT. Nevertheless, the results were in reasonable agreement with the calculations [12].

In this paper we present a measurement at a value of $Q^2 = 0.05$ GeV$^2/c^2$, halfway between the photon point and the existing electroproduction data. The present data

cover the complete azimuthal angle ϕ and allow for a Rosenbluth separation to extract the unpolarized structure functions σ_T, σ_L, and σ_{TL}. σ_{TT} was observed to be so small that only upper limits were obtained. Since the former experiments agree with the predictions of HBChPT, the clear disagreement between our results and these calculations is surprising.

Formalism and kinematics.—In the one-photon exchange approximation, the unpolarized electroproduction cross section can be written as (see, e.g., Ref. [13])

$$\frac{d\sigma(\theta_\pi^*, \phi_\pi^*)}{d\Omega' \, dE' \, d\Omega_\pi^*} = \Gamma(\sigma_T + \epsilon_L \sigma_L + \epsilon \sigma_{TT} \cos 2\phi_\pi^* + \sqrt{2\epsilon_L(1 + \epsilon)} \, \sigma_{TL} \cos \phi_\pi^*) \quad (1)$$

with the virtual photon flux Γ, photon energy ω^*, and transverse polarization ϵ, $\epsilon_L = \epsilon Q^2/\omega^{*2}$. The pion emission angles θ_π^* and ϕ_π^* are relative to the momentum transfer $\boldsymbol{q}$ and the scattering plane. Variables in the photon-proton center of mass frame are denoted with an asterisk.

In the threshold region, where only *s* and *p* waves have to be taken into account, the cross section can be further decomposed as

$$\begin{aligned} \sigma_T(\theta_\pi^*) &= (p_\pi^*/k_\gamma^*)(A + B\cos\theta_\pi^* + C\cos^2\theta_\pi^*), \\ \sigma_L(\theta_\pi^*) &= (p_\pi^*/k_\gamma^*)(A' + B'\cos\theta_\pi^* + C'\cos^2\theta_\pi^*), \\ \sigma_{TL}(\theta_\pi^*) &= (p_\pi^*/k_\gamma^*)(D\sin\theta_\pi^* + E\sin\theta_\pi^*\cos\theta_\pi^*), \\ \sigma_{TT}(\theta_\pi^*) &= (p_\pi^*/k_\gamma^*)(F\sin^2\theta_\pi^*), \end{aligned} \quad (2)$$

where p_π^*/k_γ^* is the ratio of pion CM momentum and photon CM equivalent momentum. The angular coefficients

are given by two s wave and five p wave multipole combinations [12]

$$A = |E_{0+}|^2 + \frac{1}{2}(|P_2|^2 + |P_3|^2),$$

$$B = 2\,\mathrm{Re}(E_{0+}P_1^*),$$

$$C = |P_1|^2 - \frac{1}{2}(|P_2|^2 + |P_3|^2),$$

$$D = -\mathrm{Re}(E_{0+}P_5^* + L_{0+}P_2^*),$$

$$E = -\mathrm{Re}(P_1 P_5^* + P_4 P_2^*), \tag{3}$$

$$F = \frac{1}{2}(|P_2|^2 - |P_3|^2),$$

$$A' = |L_{0+}|^2 + |P_5|^2,$$

$$B' = 2\,\mathrm{Re}(L_{0+}P_4^*),$$

$$C' = (|P_4|^2 - |P_5|^2).$$

At threshold, the s wave multipoles E_{0+} and L_{0+} are real and their energy dependence is governed by the unitary cusp caused by the two-step $\gamma^* p \to \pi^+ n \to \pi^0 p$ amplitude [14]. The p wave amplitudes P_i are real and proportional to the pion center of mass momentum p_π^*. The coefficient F is too small to be extracted in this experiment, so only the p wave combination $P_{23}^2 = (|P_2|^2 + |P_3|^2)/2$ can be determined.

Experiment.—The experiment was performed at the three-spectrometer setup of the A1 Collaboration at MAMI (see Ref. [15] for a detailed description). A liquid hydrogen target with a length of 49 mm and target walls of 10 μm Havar was used with beam currents of up to 30 μA, i.e., at a luminosity of 39 MHz/μb. For the detection of the scattered electron, spectrometer B with 5.6 msr solid angle at 15% momentum acceptance was used for the two forward angles, while spectrometer C with 22.5 msr solid angle at 25% momentum acceptance was used for the backward angle.

For the detection of the recoil proton, spectrometer A with 21 msr solid angle and a momentum acceptance of 20% was used for all settings. Table I shows the central angle and momentum settings of the spectrometers. Because of the kinematical focusing by the Lorentz boost, the full center of mass solid angle was covered within each setting up to a center of mass energy of $\Delta W = 4$ MeV above threshold.

TABLE I. Kinematical settings for the central trajectories of the spectrometers. The four-momentum transfer for all settings is $Q^2 = 0.05$ GeV$^2/c^2$

Spectr.	ϵ	E_0 (MeV)	E' (MeV)	p_p^{lab} (MeV/c)	θ_e^{lab}	θ_p^{lab}
A $\wedge$ B	0.93	855	662.3	240.0	16.8°	44.6°
A $\wedge$ B	0.72	435	263.7	233.1	38.6°	35.7°
A $\wedge$ C	0.49	330	144.0	240.0	58.5°	28.7°

All spectrometers were equipped with a detector package consisting of four layers of vertical drift chambers for position and angle reconstruction, and two layers of scintillator detectors for time-of-flight measurement and trigger. For the electron arm, the trigger was defined by the coincidence of both scintillator layers, while the low energy protons were already stopped in the first scintillator layer of spectrometer A. A halocarbon gas Čerenkov detector with a detection efficiency of 99% in this energy range was used for π^-/e^- separation, but not as part of the online trigger decision. The electron detection efficiency and calibration was checked by a measurement of elastic electron scattering.

Analysis and error estimate.—The coincidence time between electron and proton spectrometer, corrected for the flight path in the spectrometers, was determined with a resolution of 1.8 ns FWHM. This was limited by the uncertainty in the flight path due to multiple scattering of the low energy protons in the detector package of spectrometer A.

After a cut on the coincidence time, the missing mass was determined by the four-momentum subtraction of incoming and outgoing particles, i.e., by $m_{\mathrm{miss}}^2 = (e_{\mathrm{in}} + p_{\mathrm{in}} - e_{\mathrm{out}} - p_{\mathrm{out}})^2$. A missing mass resolution of 2.0 MeV/c^2 was achieved, again limited by the multiple scattering of the low energy protons.

The phase space was calculated in a Monte Carlo simulation including resolution, multiple scattering, energy loss, and radiative corrections, the later based on the formulas of Ref. [16].

The background contribution was determined by a cut in the coincidence time spectrum. Since the modest missing mass resolution allowed only a loose cut of ± 3 MeV/c^2 around the π^0 mass, the signal to background ratio was ≈ 1 averaged over the acceptance. The background, however, could be determined with a timing cut of 10 times the width of the cut for the true events, leading to no significant contribution to the statistical error by the background subtraction.

The systematic error is dominated by different effects at low and high energies. For the lowest energy bin, the calibration of the momentum of the electron arm is crucial, since assuming a too high electron momentum leads to a smaller photon momentum and a smaller total CM energy, so that some of the events are shifted below threshold. This error was estimated by varying the central momentum of the electron arm in the analysis. For the lowest energy bins we assumed $\delta\sigma/\sigma = 20\%$ error at $\Delta W = 0.5$ MeV and 10% at $\Delta W = 1.5$ MeV.

For the higher energy bins, the acceptance of the proton arm is not uniform, and a few angular bins are multiplied by large phase space correction factors. This contribution to the systematic error can be estimated by varying software cuts on the acceptance.

Compared to these two effects, the contribution of the efficiency and other corrections can be neglected. Over

all, we estimated an error of $\delta\sigma/\sigma = 5\%$ (3%) at $\Delta W = 2.5$ MeV (3.5 MeV).

After determining the twofold cross section $\sigma(\theta_\pi^*, \phi_\pi^*)$ for the three epsilon points, a fit with the known ϕ_π^* dependence [Eq. (1)] was performed in each θ_π^* bin to extract $\sigma_0(\theta_\pi^*) = \sigma_T(\theta_\pi^*) + \epsilon_L \sigma_L(\theta_\pi^*)$ and $\sigma_{TL}(\theta_\pi^*)$.

Results.—Figure 1 shows the differential cross section for four energy bins at the medium epsilon point in comparison with the predictions of HBChPT [12] and a phenomenological model (MAID) [17]. The complete data set can be obtained from our web site. Figure 2 shows the transverse-longitudinal interference structure function extracted as weighted average from all three settings.

In order to extract the multipole amplitudes, a fit using Eq. (3) with the assumption of constant real s wave multipoles (i.e., E_{0+}, L_{0+} constant in energy) and real p wave multipoles proportional to the pion CM momentum ($P_i = p_\pi^* \hat{P}_i$ with $\hat{P}_i$ constant in energy) was performed, indicated by a solid line in the figures. These assumptions are not exactly valid, since a variation of $\approx 5\%$ in the total s wave amplitude is expected due to the unitary cusp [12,14], but the statistical significance of the data is not sufficient to resolve this variation. The extracted fit parameters are presented in the first row of Table II.

It is important to note, that a least squares fit cannot give a real picture of the sensitivity of the data to the multipole amplitudes. The data set is dominated by the systematic error and thus violates a fundamental precondition of Gaussian distributed errors for a χ^2 fit.

To compare the present result with former experiments in a consistent way, the same fit was performed to the data sets at $Q^2 = 0.1$ GeV$^2/c^2$, which are believed to be more or less consistent with HBChPT on the cross section level. The fit results are included in Table II and differ from the multipole amplitudes quoted in the corresponding references [9,11], which were extracted using model assumptions.
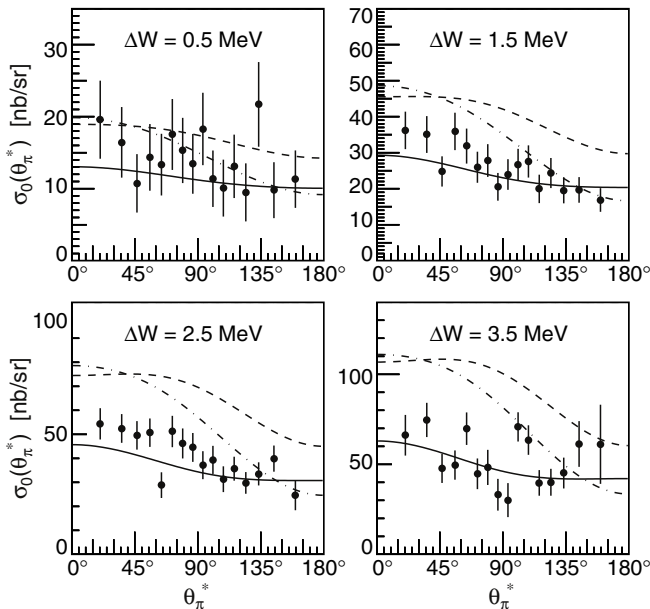
Figure 3 shows the unpolarized total cross section $\sigma_{\text{tot}} = \int(\sigma_T + \epsilon_L \sigma_L)\,d\Omega$ as a function of Q^2 to further illustrate the discrepancy between the currently available data and the calculations in a model independent manner. While the photo production data could be described by both HBChPT and MAID, the strongest deviation appears at the Q^2 value of the present experiment, while already at $Q^2 = 0.1$ GeV$^2/c^2$, where the parameters of HBChPT were determined, a deviation from the HBChPT calculation of up to 20% appears. The disagreement with the MAID model is even larger.

From the fit parameters quoted in Table II one can see that the major part of the discrepancy comes from the large p wave multipole combination P_{23}^2. This is a serious problem for the prediction of HBChPT, since this combination is already fixed by the photoproduction data and cannot be adjusted by varying the free parameters of the calculation to the current order. The strong curvature in the Q^2 dependence of Fig. 3 clearly indicates that higher orders in Q^2 have to be included in the p wave description.

In order to check the surprising result of our experiment, we repeated our differential cross section measurement for the highest epsilon (0.92) in an independent experiment. The result of this experiment agreed with the present experiment within the errors. In addition, since these results rely on the quality of the simulation and phase space

FIG. 1. Differential cross sections for the first 4 MeV above threshold for the virtual photon polarization $\epsilon = 0.72$. The solid line represents a fit with the assumption of only s and p waves contributing, the dashed and dash-dotted lines represent the predictions of HBChPT [12] and MAID [17].
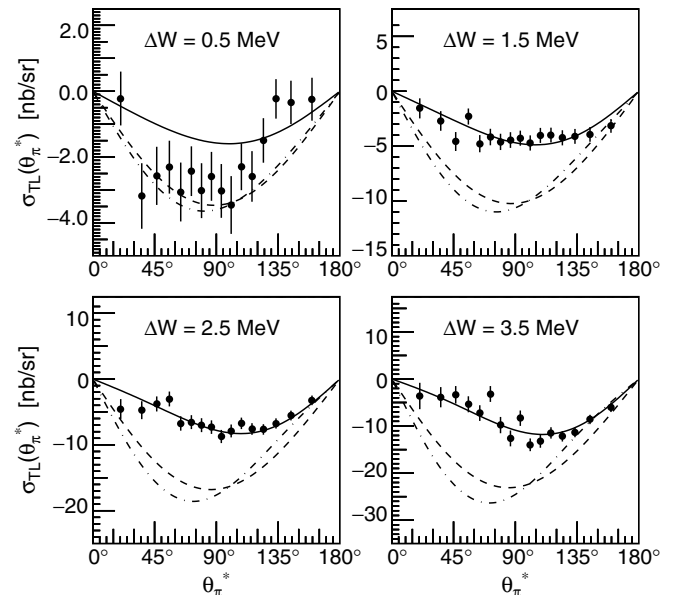
FIG. 2. The transverse-longitudinal interference structure function, determined as weighted average of all three settings for ϵ. Assignment of lines as in Fig. 1.

TABLE II. Extracted multipole amplitudes in comparison with the threshold values of HBChPT [12] and MAID [17]. The AmPS [10] value for $|L_{0+}|$ was extracted from their value for $a_0 \approx \epsilon_L |L_{0+}|^2$. For the AmPS [9] fit L_{0+} was fixed, since no Rosenbluth separation was performed.

	Q^2 (GeV^2/c^2)	E_{0+} ($10^{-3} m_\pi^{-1}$)	L_{0+}	$\hat{P}_{23}^2$ ($10^{-6} m_\pi^{-4}$)	$\hat{P}_1$	$\hat{P}_4$ ($10^{-3} m_\pi^{-2}$)	$\hat{P}_5$
Fit	0.05	0.57 ± 0.11	-1.29 ± 0.02	100 ± 3	12.0 ± 0.3	0.29 ± 0.33	-1.9 ± 0.3
AmPS [10]			$(-)1.57 \pm 0.96$				
ChPT		0.27	-1.55	353	16.5	-0.72	-0.2
MAID		0.76	-1.4	250	15.0	-1.75	1.9
MAMI [6]	0	-1.33		111	9.5		
ChPT		-1.14	-1.70	105	9.3	-0.6	-0.2
MAID		-1.16	-1.29	95	9.3	-3.0	2.2
MAMI [11]	0.1	0.58 ± 0.18	-1.38 ± 0.01	573 ± 11	15.1 ± 0.8	-2.3 ± 0.2	0.1 ± 0.3
AmPS [9]		1.99 ± 0.3	-1.33 (Fixed)	526 ± 7	16.4 ± 0.6	-1.0 ± 0.4	-1.0 ± 0.4
ChPT		1.42	-1.33	571	20.1	-0.6	-0.1
MAID		2.2	-1.12	315	17.1	-1.1	1.4

integration program, a new, completely independent code was written to check the phase space integration.

In summary, it appears that there is a significant discrepancy between HBChPT and phenomenological models on the one hand and the experimental data on the other hand. However, an inconsistency in the different electroproduction data sets, which were all taken in separate experiments, cannot be excluded. As mentioned above, a repeated measurement at $Q^2 = 0.05$ GeV^2/c^2 and $\epsilon = 0.92$ at MAMI confirmed our result. We plan to further explore the Q^2 dependence in a future experiment. An independent measurement at the Jefferson Lab in the same Q^2 range is also planned [18].

*Email address: Merkel@kph.uni-mainz.de
http://wwwa1.kph.uni-mainz.de/
†Present address: TU München, Garching, Germany.
‡Present address: INFN Sezione di Pisa, Pisa, Italy.
§Present address: TRIUMF, Vancouver, B.C., Canada.
‖Present address: University of Glasgow, Glasgow, U.K.
¶Present address: M.I.T., Cambridge, MA 02139.

[1] S. Weinberg, Physica (Amsterdam) 96A, 327 (1979); A. W. Thomas and W. Weise, The Structure of the Nucleon (Wiley-VCH, Berlin, 2001).
[2] Chiral Dynamics: Theory and Experiment III, edited by A. M. Bernstein, J. L. Goity, and U.-G. Meißner (World Scientific, Singapore, 2001).
[3] V. Bernard et al., Nucl. Phys. B383, 442 (1992).
[4] R. Beck et al., Phys. Rev. Lett. 65, 1841 (1990).
[5] M. Fuchs et al., Phys. Lett. B 368, 20 (1996); A. M. Bernstein et al., Phys. Rev. C 55, 1509 (1997).
[6] A. Schmidt et al., Phys. Rev. Lett. 87, 232501 (2001).
[7] J. C. Bergstrom, Phys. Rev. C 44, 1768 (1991).
[8] J. C. Bergstrom et al., Phys. Rev. C 53, R1052 (1996).
[9] H. B. van den Brink et al., Phys. Rev. Lett. 74, 3561 (1995).
[10] T. P. Welch et al., Phys. Rev. Lett. 69, 2761 (1992).
[11] M. O. Distler et al., Phys. Rev. Lett. 80, 2294 (1998).
[12] V. Bernard, N. Kaiser, and U.-G. Meißner, Nucl. Phys. A607, 379 (1996); A633, 695(E) (1998).
[13] D. Drechsel and L. Tiator, J. Phys. G 18, 449 (1992).
[14] A. M. Bernstein, Phys. Lett. B 442, 20 (1998).
[15] K. I. Blomqvist et al., Nucl. Instrum. Methods Phys. Res., Sect. A 403, 263 (1998).
[16] L. W. Mo and Y.-S. Tsai, Rev. Mod. Phys. 41, 205 (1969).
[17] D. Drechsel et al., Nucl. Phys. A645, 145 (1999); S. S. Kamalov et al., Phys. Lett. B 522, 27–36 (2001).
[18] R. Lindgren et al., Experiment E01-014, JLab, 2001.

FIG. 3. The total cross section σ_{tot} versus Q^2, at a value of $\epsilon = 0.8$. The solid (dashed) line is the prediction of ChPT (MAID), data points at $Q^2 = 0$ and 0.1 GeV^2/c^2 from [6,11].